#179

Reprinted from

surface science

Surface Science 426 (1999) 336–344

Quantum coherence effects in the scanning tunneling microscope: a simple interpretation of contact resistance experiments

F. Biscarini [a,*], V.M. Kenkre [b]

[a] *CNR-Istituto di Spettroscopia Molecolare, Via P. Gobetti 101, I-40129 Bologna, Italy*
[b] *Center for Advanced Studies and Department of Physics and Astronomy, University of New Mexico, Albuquerque, NM87131, USA*

Received 18 September 1998; accepted for publication 27 January 1999

ELSEVIER

ELSEVIER

Surface Science 426 (1999) 336–344

surface science

www.elsevier.nl/locate/susc

Quantum coherence effects in the scanning tunneling microscope: a simple interpretation of contact resistance experiments

F. Biscarini [a,*], V.M. Kenkre [b]

[a] *CNR-Istituto di Spettroscopia Molecolare, Via P. Gobetti 101, I-40129 Bologna, Italy*

[b] *Center for Advanced Studies and Department of Physics and Astronomy, University of New Mexico, Albuquerque, NM87131, USA*

Received 18 September 1998; accepted for publication 27 January 1999

Abstract

Quantum coherence effects that arise in the scanning tunneling microscope (STM) when the tip is brought in close proximity to the substrate are addressed on the basis of a recently reported theory in which a continuous transition from an incoherent regime at large gap distances to a coherent regime at short distances is described by means of electron propagators. A simple model of the STM junction is introduced, and is shown to provide a simple and intuitive explanation for the appearance of plateau and a jump in the current characteristics. © 1999 Elsevier Science B.V. All rights reserved.

Keywords: Adatoms; Contacts; Models of non-equilibrium phenomena; Platinum; Quantum effects; Scanning tunneling microscopy; Silver

1. Introduction

When the tip of a scanning tunneling microscope (STM) is brought in close proximity to the sample, the tunneling current, I, exhibits a spatial variation with the gap distance, z, which is counter-intuitive on the basis of semi-classical theories [1–4]. Early STM measurements on a Ag film showed a plateau in the distance dependence of the tunneling current followed by a sudden jump as the tip approaches the sample [5,6]. Similar effects were observed on various metal surfaces [7,8]. Plateau and jump have been ascribed to the onset of quantized conduction through an orifice junction formed by one or few atoms at the tip apex in contact with the substrate (Sharvin regime), leading to the collapse of the potential barrier between the tip and substrate below the Fermi level, resulting in ballistic electron transport across the junction [9]. The finite size of the opening would lead to a discrete number of channels whose transverse momentum matches the lateral boundary conditions, each channel contributing a quantum of conductance $2e^2/h$ [10–12] and producing jumps in the I–z characteristics. In these experiments [5–8] the tip merely approaches the sample, and no mechanical contact probably occurs. Therefore, we term these experiments [5–8] 'before-contact'. In another distinct group of experiments [13–20], mechanical contact between the tip and sample does occur prior to the observation of the steps. This second group has been discussed via simulations of the tensile behaviour of the elongating

* Corresponding author. Fax: +39 051-6398539.
E-mail address: fabio@ism.bo.cnr.it (F. Biscarini)

PII: S0039-6028(99)00292-7

neck [14,18,21] and via the theory of ballistic transport through narrow junctions [22–25], and we do not address them in this paper.

Our present work is aimed at a 'before-contact' type of experiments. Most of the theoretical work on these experiments has focused on the electronic features, and a model junction consisting of two metal reservoirs connected by a single atom has often been used. It has been argued [6,26] that, when the tip is in the close proximity of the surface, the exchange-correlation potential causes the barrier to collapse at distances already larger than the bond length and the current to reach a saturation plateau. The plateau is a property of the detailed chemical nature of the tip apex [26,27], and the changing sign of the overlap of the wave-functions of tip and sample as the gap decreases has been postulated as its possible origin [28]. Other electronic structure theories [29–31] have also reproduced the characteristics before contact, but none of them has been able to predict the occurrence of the jumps. Only molecular dynamics simulations of the reorganization processes at the STM junction have been able to yield jumps due to mechanical instabilities and atom motion at the tip–sample interface [32].

Although these results have shed light on the electronic and geometrical structure origin of the characteristics in the short-range regimes, an open question has remained: how to describe within a single framework the three different regimes (viz. tunneling, plateau, jump) observed in the I–z characteristics of the 'before-contact' experiments. In most of the previous theoretical studies, it has been implicitly assumed that the conductance arises by a simple sum of contributions of individual channels [16]. The issue of quantum interference when the tip is brought near to the substrate is the focus of the present paper. We show that the onset of interference yields a rapid, but not discontinuous, increase in the I–z characteristics, which resembles the first jump in the characteristics. The substrate atom adsorbed at the tip apex is considered to be responsible for the observed features, and the occurrence of both plateaux and current jumps arises from a competition between direct transfer rates for electron and interference contributions. In this framework, the asymmetry in the chemical nature of the junction is of fundamental importance. Our results suggest that, by accounting properly for the interference effects, one might be able to describe the three regimes (tunneling, plateau, jump) observed in I–z 'before contact' experiments without invoking atom motion at the interface or mechanical instabilities as the origin of the jumps.

2. The model

The simplified model STM junction consists of three (Wannier) site states representing the tip, substrate and tip apex (labeled, respectively, T, S and A). On the basis of these states, the Hamiltonian reads

$$\boldsymbol{H}=\begin{pmatrix} E_{\mathrm{T}} & V_{\mathrm{TA}} & 0 \\ V_{\mathrm{TA}} & E_{\mathrm{A}} & V_{\mathrm{SA}} \\ 0 & V_{\mathrm{SA}} & E_{\mathrm{S}} \end{pmatrix}, \tag{1}$$

where the Vs are the matrix elements, and the Es are the site energies. The tip apex, A, does not change its distance from the tip as the tip–substrate distance is varied, the change in the STM configuration being through the substrate–apex matrix element V_{SA} (the direct tip–substrate matrix element, V_{ST}, is taken to be vanishing for simplicity). The STM effective resistance, R_{eff}, of such a three-site junction can be calculated in terms of our earlier theory of the STM [33,34]:

$$R_{\mathrm{eff}} \propto \int_0^\infty \mathrm{d}t[\Pi_{\mathrm{TT}}(t)+\Pi_{\mathrm{SS}}(t)-\Pi_{\mathrm{TS}}(t)-\Pi_{\mathrm{ST}}(t)]. \tag{2}$$

Here, the electron propagator, Π_{mn}, represents the probability of finding the electron on the site m at time t given an initial placement of the electron at site n [33]. The effective resistance, R_{eff}, depends on the value of the ratios of the matrix elements V to an incoherence parameter, α, which describes bath interactions, alternatively, the energetic disorder in the STM junction. When $\alpha=0$, the carrier motion is fully coherent, whereas for a large α, it becomes incoherent. By tuning the ratio of the

interstate matrix elements V to α (which happens as the tip is moved towards the sample), the character of the motion can be made to change continuously between the two limiting regimes.

If $E_T=E_S=E_A$, Ref. [33] yields, with the replacement of the label M by A in the present paper and the transposition of labels T and S

$$R=\left[1+\left(\frac{V_{TA}}{V_{SA}}\right)^2\right]+\left(\frac{V_{TA}}{\alpha}\right)^2\left[\frac{V_{SA}}{V_{TA}}-\frac{V_{TA}}{V_{SA}}\right]^2. \quad (3)$$

We suppress unimportant constants. In Fig. 1, R is plotted as a function of V_{SA} for different values of V_{TA}, as shown, the value of a being held constant. The plot corresponds to the tip being moved closer to the substrate as V_{SA} is increased. In analogy with the apparent STM barrier height, ϕ_a [3,4] defined as

$$\phi_a=0.952\left[\frac{\partial \ln I}{\partial z}\right]^2, \quad (4)$$

where ϕ_a is in electron-volts, the current, I, is in nanoamps and the distance, z, is in angstroms, the dimensionless apparent barrier ϕ_a^* is

$$\phi_a^*=\left[\frac{d\ln(1/R)}{d\ln(V_{SA})}\right]^2.$$

In Eq. (4), the quantity whose logarithm differentiated is the current, whereas in Eq. (5 is the reciprocal of the effective resistance give Eq. (3). The derivative is with respect to the distance in Eq. (4) and also in Eq. (5) if tunneling matrix element has a simple exponen dependence on the gap distance. Eq. (5) is t an appropriate representation of Eq. (4) to add the qualitatives of the dependence of the bar height on distance. Three distinctive features apparent in Figs. 1 and 2. In Fig. 1, we obse (1) the occurrence of a resistance minimum a critical tip–substrate distance, (2) the depende of the shape and location of the minimum on value of V_{TA} , and (3) the lack of dependence resistance on V_{TA} for small V_{SA}, i.e. for large ti substrate distances. Feature (1) corresponds, our plot of the effective barrier height in Fig. 2, the vanishing of ϕ_a^* for certain values of the su strate–apex interaction (consequently of the g distance). The correspondence of feature (2) similarly clear in the shapes of the curves in Fig. Feature (3) is represented in Fig. 2 by the co vergence of the various curves to the incoherer

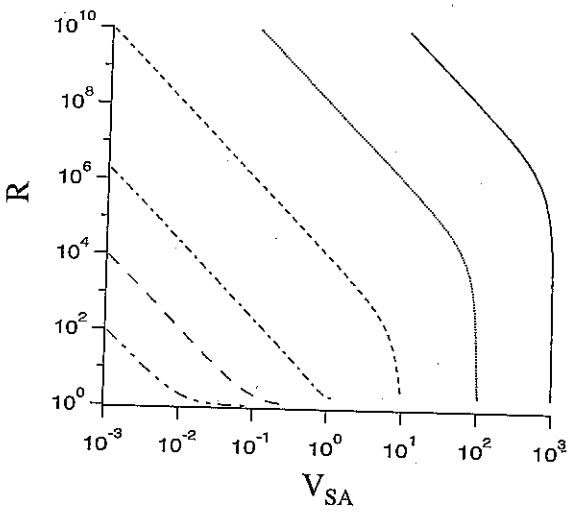

Fig. 1. Resonant three-site model. Dimensionless effective resistance vs. matrix element V_{SA} for a different strength of interaction $V_{TA}=0.01$ (double dot-dash), 0.1 (large dash), 1 (dot-dash), 10 (small dash), 100 (dots), 1000 (solid). In this and other figures, the matrix elements are in units of α, and the curves are interrupted at the configuration of minimum resistance.

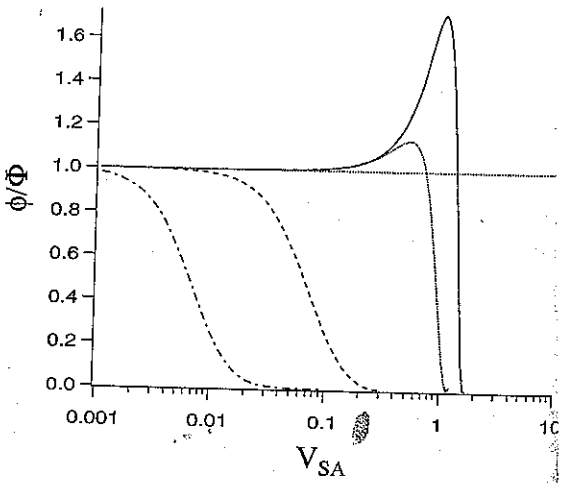

Fig. 2. Resonant three-site model. Dimensionless apparent bar rier height vs. V_{SA} for a different strength of interaction $V_{TA}=0.01$ (dot-dash), 0.1 (dash), 1 (dots), 1.5 (solid).

ırrier ϕ_a^* is

(5)

ty whose logarithm is
ıt, whereas in Eq. (5), it
ective resistance given in
with respect to the gap
also in Eq. (5) if the
has a simple exponential
listance. Eq. (5) is thus
tion of Eq. (4) to address
ependence of the barrier
e distinctive features are
2. In Fig. 1, we observe
resistance minimum at a
ance, (2) the dependence
ı of the minimum on the
ne lack of dependence of
all V_{SA}, i.e. for large tip–
ture (1) corresponds, in
barrier height in Fig. 2, to
certain values of the sub-
(consequently of the gap
ndence of feature (2) is
pes of the curves in Fig. 2.
ed in Fig. 2 by the con-
curves to the incoherent,

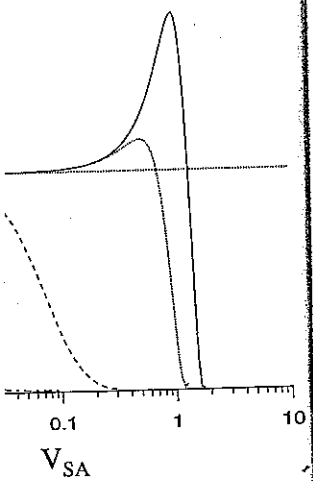

odel. Dimensionless apparent bar-
different strength of interaction
ısh), 1 (dots), 1.5 (solid).

i.e. a large gap separation, limit ($\phi_a/\Phi=1$ in Fig. 2, where Φ is the actual work function of the metal surface). The observed plateaux in the current (equivalently in the effective resistance as in Fig. 1) correspond in Fig. 2 to the smooth and relatively large regions of near-zero values of ϕ_a^* whereas the observed jumps in the current (equivalently the spikes in Fig. 1) are represented by sudden, rather than smooth, drops to zero. Also, the curves showing the jumps in the current have a point of inflexion represented by the rise of the ϕ_a^* curves above the large-gap value, Φ^*. Such a behaviour can be found also in other experimental work [7], and analysis (see fig. 3 of Ref. [9], and figs. 3 and 4 in Ref. [35]) where it appears related to the local character of the surface potentials used in their calculations. A large enhancement in the apparent barrier at distances near the contact arises in the square barrier as the transmission probability undergoes a transition from a smooth to an exponential decay [35]. In our present analysis, the observed features arise from the interplay between the two contributions to the effective resistance (4): the symmetrical/incoherent and asymmetrical/coherent terms [33]. The former is responsible for the plateau at a short distance in Fig. 1 and is dominant in the incoherent regime. The latter contribution becomes relevant under coherent transport conditions, and causes the rapid decrease in effective resistance as $V_{SA}/V_{TA}\to 1$.

The resonant model expression (3) is thus able to reproduce both the plateau and the jump characteristics (and even the rise in the effective barrier height above the large gap separation value) *but only in different parameter cases*. In order to account for their coexistence, it is necessary to examine off-resonant models. Having analysed in detail three cases with a single on-site energy mismatch, respectively of the substrate, apex and tip, we have found that only the third case in which a substrate atom is adsorbed at the tip apex is successful in predicting the coexistence of the jump and the plateau. The effective resistance, R, is calculated by multiplying the integral Eq. (2) by α. The outcomes are plotted in Fig. 3.

In Fig. 3a, we take a high degree of coherence in electron transport, specifically a value that is low enough such that $V_{TA}=100$ in units of α, and show the dependence of the I–z characteristics on the energy mismatch ω. For $\omega/V_{TA}\ll 1$, the characteristics resemble the resonant case, and the maximum conductance decreases as the mismatch increases. As $\omega/V_{TA}\approx 1$, the slope decreases as the tip approaches the substrate: in the far distance regime, the conductance is proportional to V_{SA}^2 as expected for tunneling, and the decrease of the power exponent is symptomatic of coherent transport [33]. The slope decrease has been reported in several experimental STM studies [6–8]. At larger ratios ($\omega/V_{TA}>1$), the tunneling regime ends on a plateau, and the separation range, where the conductance is insensitive to the distance, grows with the energy mismatch. The conductance rises again at the end of the plateau. There is no true discontinuity, although the relevant spatial range of V_{SA} spans less than one order of magnitude. This would correspond to just a fraction of an angstrom. It is also interesting to note that the occurrence of the spike in the model corresponds to the tip position beyond the symmetric configuration ($V_{SA}=V_{TA}$), corresponding to V_{SA} being close to the energy mismatch with the tip. This suggests that the current jump is the result of either one of the split levels arising from the apex–substrate interaction coming into resonance with the mismatched tip level [26].

Fig. 3b shows the evolution of the I–z characteristics at a given energy mismatch and for different degrees of coherence measured by the value of V_{TA} in units of α. The key quantity that determines the plateau onset and the sharp rise in proximity of the contact point is the ratio ω/V_{TA} rather than the absolute coherence value. A scaling relationship of the I–z characteristics as a function of ω/V_{TA} is seen to exist from Fig. 3c. Curves with the same ω/V_{TA} and different V_{TA} can be collapsed onto a universal curve if displayed as a function of V_{SA}/V_{TA}. In other words, a given pair of tip and substrate yields the same characteristics in the mismatched configuration independently on the degree of coherence. As a consequence, the onset of the plateau region shifts towards a smaller V_{SA} (larger separation) as the degree of coherence decreases. This might imply that even a modest approach distance from the set-point position yields saturation in the current [8]. Fig. 3d shows the effect of changing the α value while maintaining

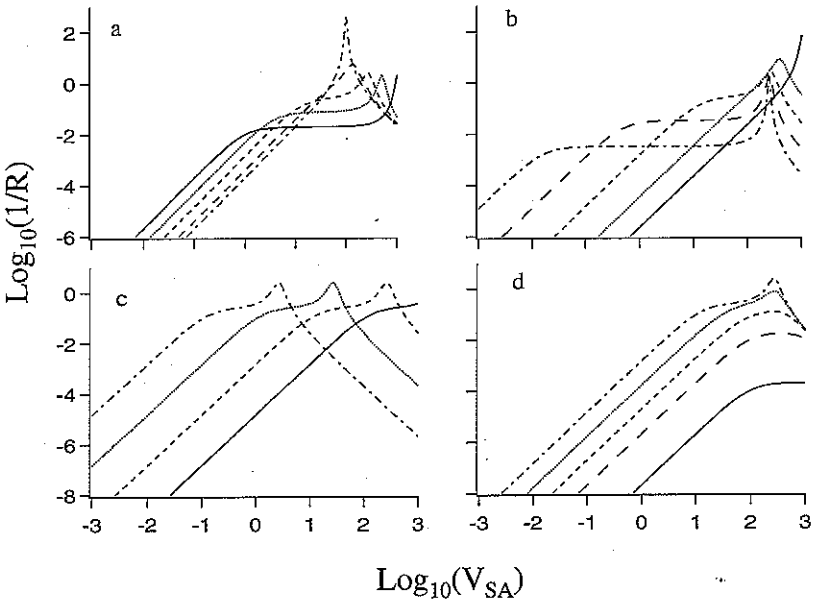

Fig. 3. Dimensionless effective conductance vs. V_{SA} for the off-resonance three-site system with mismatched tip energy, ω: $V_{TA}=100$ and $\omega=10$ (dot-dash), 100 (large dash), 250 (small dash), 500 (dot), 1000 (solid) in units of α; (b) $\omega=250$ a $\mathrm{Log}_{10}(V_{TA})=1$ (dot-dash), 1.5 (large dash), 2 (small dash), 2.5 (dot), 3 (solid) , matrix elements in units of α; (c) constant ra $\omega/V_{TA}=2.5$ and $V_{TA}=1$ (dot-dash), 10 (dot), 100 (dash), 1000 (solid) in units of α; (d) constant ratio $\omega/V_{TA}=2.5$, $V_{TA}=100/\alpha$, a $\log_{10}(\alpha)=0$ (dot-dash), 1 (dots), 1.25 (small dash), 1.5 (large dash), 2 (solid).

the relative matrix elements fixed. This effect is implemented by rescaling the Hamiltonian as $V_{TA}=100/\alpha$ while maintaining $\omega/V_{TA}=2.5$. For $\alpha\leq 1$ (coherent conditions), the I–z characteristics saturate to the curve with plateau and jump (dot-dashed line). As α increases (less coherence), the plateau shrinks, and the jump fades out. For yet larger α values, only a featureless maximum appears, as in the incoherent resonant case. Thus, the coexistence of the jump and the plateau is seen as a result of the coherent transport conditions.

3. Comparison to experimental data

A comparison between the experimental data of Gimzewski and Möller [5,6] and our theoretical model is shown in Fig. 4. In the experiment, the initial position, z_0, of the tip is set by imposing a 1-nA tunneling current for a 20-mV bias voltage. The characteristics are recorded as a function of the approach distance z_0–z. In the first curve (Fig. 4a), the current rises about 2.5 orders of magnitude on the 4.73-Å distance range befo contact. The characteristics exhibit a small platea in close proximity to the contact point, whi spans approximately 0.25 Å. In the second expe ment (reported in Ref. [6]), the characteristi shown in Fig. 4b exhibit both a large plateau (sp of approximately 2 Å) and a jump. According the model calculations shown in Fig. 3, these cha acteristic features appear upon coherent transpc conditions, so we choose $V_{TA}=100$ in units of and we improve the fitting by a slight offset of t $\log_{10}(V_{SA})$ axis, which is equivalent to a sm adjustment of V_{TA} (see Fig. 3c). Note from Fig. that a small plateau, as in the experimental chara teristics in Fig. 4a, implies an energy mismatch comparable to the relevant matrix element V_T Then, in Fig. 4a, we superimpose the theoretic curve for the three-site off-resonance model calc lated for $\omega/V_{TA}=1.1$, and we set the range for t matrix element V_{SA} in such a way that the theore cal conductance undergoes a change of four orde of magnitude, and its maximum coincides with t observed jump at the experimental contact poin

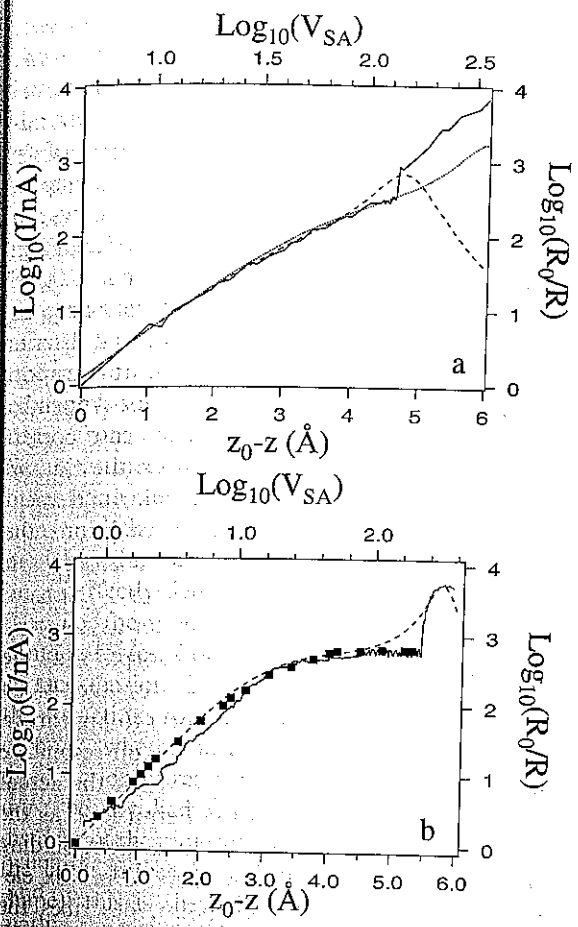

Fig. 4. Comparison between experimental current vs. distance towards the surface curves (solid line, left and bottom axes) and theoretical results of the off-resonance three-site model (dashed line, right and top axes). The experimental data are taken from (a) Ref. [5] and (b) Ref. [6], the markers are density functional calculations from Ref. [6]. The parameters of our theoretical curves are $V_{TA}=100$ in units of α and (a) $\omega/V_{TA}=1.1$ (dashes), 1.4 (dots) and (b) $\omega/V_{TA}=2.5$, respectively.

Our theoretical I–z characteristics reproduce the experimental data in the tunneling regime and the change of slope at the onset of the small plateau before contact. Although the sharp jump at contact is not reproduced quantitatively, the model predicts that the conductance will increase faster when the tip is in proximity (closer than 0.5 Å) to the contact point. The increase in experimental current signal after the jump is probably due to the increased number of atoms in proximal interaction, as suggested by the significant hysteresis upon tip retraction reported in [5]. In any case, our model cannot account for the trend observed beyond the maximum conductance. Using a slightly larger energy mismatch, $\omega/V_{TA}=1.4$, and relaxing the condition on the maximum conductance, we can fully reproduce the I–z characteristics, including the plateau and the current rise beyond the jump (dotted curve in Fig. 4a). It is interesting to compare this result with the saturation of the current beyond the jump as predicted by a different tight-binding model [29].

Fig. 4b shows a comparison between the experimental data, the density functional calculation [6] and our model calculation for $\omega/V_{TA}=2.5$. The energy mismatch is determined by matching both the contact point and the onset of the plateau. Far from contact, the characteristics are dominated by tunneling from the tip apex to the substrate, whose distance determines the effective gap. The agreement is excellent throughout the range, and the current increase occurs when $V_{SA}\approx V_{TA}$, which corresponds to the tip being within 0.4 Å from the experimental jump. Interestingly, the configuration for which the maximum current is achieved is not symmetrical. From the equivalence between the bottom and top axes, it appears that the skewed configuration at the maximum corresponds to a difference in bond length of 0.5 Å, which is comparable to the value obtained from molecular dynamics simulations of the jump-to-contact process [15].

Our model calculations suggest that the two experimental curves arise from different tips. If we identify the energy mismatch ω as the effective difference in the work function between the tip and substrate, and the matrix element V_{TA} as the interaction between the apex adatom with the tip states, we can extract useful parameters from the experiment. The work function difference between Ir ($\Phi=5.7$ eV) and polycrystalline Ag ($\Phi=4.6$ eV) is $\omega=1.1$ eV; hence, ω/V_{TA}, which fits the experimental data, yields the matrix element values $V_{TA}\approx 1$ eV (dashed curve in Fig. 4a) and $V_{TA}\approx 0.4$ eV, respectively. On the other hand, the decay of the length of V_{SA} estimated from the comparison of the matrix element, V_{SA} and the spatial ranges in Fig. 4, is comparable in the two

cases: in Fig. 4a, one order of magnitude decrease of the matrix element V_{SA} corresponds approximately to a 3.2 Å gap increase, and the inverse decay length calculated from the linear dependence between $\log_{10}(V_{SA})$ and z_0-z is 0.5 $Å^{-1}$. Similar considerations in Fig. 4b yield an inverse decay length of 0.45 $Å^{-1}$. Thus, we infer that the chemical nature of the tip apex is similar in both cases and that the different ratios might be ascribed to a different structure of the tip, which is reflected in the different V_{TA} value. The smaller V_{TA} value in the latter case might imply that the local environment of the tip apex is made of fewer atoms with respect to the former case, for instance, for a sharp tip. This result is consistent with the earlier hypothesis [31] that *sharp tips would produce plateaux*, whereas blunt tips would produce a monotonic increase in current with distance. Although the three-site model does not contain the tip structure, this information is implicitly embedded in the value of the matrix element V_{TA}. We have performed calculations on larger clusters of atoms as models of the STM junction and have found that the behaviour exhibited by the characteristics of the three-site model is indeed preserved.

4. Discussion

Our analysis suggests that the plateau and the jump in the *I–z* characteristics are a result of coherent transport through a localized state at the tip's apex which is in resonance with the substrate, e.g. an Ag atom on the Ir tip in the experiment in Ref. [5]. This is supported by the fact that choosing either different sequences of localized states or a different degree of coherence in the electron motion does not yield all the features observed experimentally. The physical picture emerging from our model is consistent with several previous experimental and theoretical studies. For instance, substrate atoms are adsorbed at the tip apex in actual STM conditions during in-situ sharpening of the tip, which is performed either by indentation of the tip into the substrate, or by field desorption. Localized states, as in weakly bound adatoms, have been observed at the tip apex [36,37]. These aspects are qualitatively embodied in the essential features of our model and in the choice of relevant parameters. Moreover, the conclusion from the fitting of our model to independent experimental data is consistent with previous hypotheses regarding the origin of the characteristics in terms of tip apex chemical nature and geometry. While simplistic from the electronic structure point of view, our model treats rigorously interference effects that might exist among conductance channels.

Our model does not explicitly take into account the breakdown of the surface potential barrier [3,6,9], which causes the onset of ballistic transport across the junction. In chain models (see Appendix A), ballistic transport in a resonant case corresponds to the matrix element between the tip and substrate matching the intersite matrix element within each electrode. Under such conditions, the junction (where the resistance is higher) disappears, and transport occurs in a continuous 1-D chain, as in Bloch states. In the case of an asymmetric junction and in the case of physisorption at the tip apex, one expects $V_{SA} > V_{TA}$ for the Bloch condition (hence ballistic transport) to appear. In fact, the minimum resistance of the off-resonance model occurs at $V_{SA} \approx \omega \geq V_{TA}$. Even if the actual barrier height drops below the Fermi level as the tip approaches the substrate, in a tight-binding formulation, there is still an effective matrix element which, at the contact point, describes the conduction through a Ag wire, for example. The increase in conductance before the peak suggests that the transition from tunneling to ballistic transport is smooth, similarly to the actual breakdown of the barrier [9].

In our picture, the plateau arises because the contribution to the conductance from the gain in the matrix element V_{SA} is exactly canceled by destructive interference (see the curves in Fig. 3a with respect to the resonant case in the intermediate range). In the long-distance regime (small V_{SA}), the interference terms become small and positive, causing the decrease to follow the well-known V_{SA}^2 relation. Finally, the largest meaningful V_{SA} corresponds to the maximum conductance. Less coherent conditions (i.e. larger bath interactions) can push the onset of the resonance to larger V_{SA}. Thus, the maximum conductance might not always be experimentally accessible because of

instabilities. The important result that can be inferred from our model is that the asymmetry in the junction (either chemical or geometrical) is important in order to yield the plateau and the first jump.

In Appendix A, we show that our model predicts that a quantum of conductance $2e^2/h$ is the maximum conductance that can be observed for fully coherent 1-D transport, consistent with the well-known result of Landauer's formula for a single conductance channel [10,11]. Furthermore, we find that for a junction consisting of a chain of $M+1$ atoms, with $M>1$, the minimum resistance increases as $\approx\ln(M)$. This intriguing result seems to be at variance with the result of Ref. [38]. The discrepancy originates in our artificial separation of the intermediate state from the rest of the junction, which is coupled directly to the reservoirs. However, in our opinion, the most important reason lies in the breakdown of the assumption in [38] of a very narrow intermediate potential well with respect to the wavefunction spread. This argument has been discussed in Refs. [9,26] in order to explain how the saturation resistance through one atom becomes larger than the ideal 12.9 kΩ value (inverse of $2e^2/h$). In our model, when the coupling V between the intermediate site and tip and substrate is comparable to the coupling within the chain (see Appendix A), the root-mean-square displacement from the intermediate site is proportional to V. Thus, there is never a spatial localization on the intermediate site, and the conditions in Ref. [38] do not hold. For a three-site system, our model predicts the minimum resistance to be $R_{\rm eff}=\frac{4}{3}R_0\approx 17$ kΩ, in accidental agreement with ≈ 16.4 kΩ measured at the conductance jump in Ref. [6], and for an off-resonance condition, we expect an even larger value, in agreement with the conclusions of Refs. [6,26,27,36].

An important result of our model is that only in a regime of negligible bath interactions (i.e. large Vs in units of α) would the characteristics exhibit a rapid change in slope at the contact point (viz. $V_{\rm SA}\approx V_{\rm TA}$ in the resonant case and $V_{\rm SA}\approx\omega\geq V_{\rm TA}$). In conclusion, the 'jump' is the result of coherent transport on contact, and not just the signature of contact. The transport on contact *is not* necessarily coherent, and in the incoherent case, the conductance will not show a rapid increase at the contact point.

Acknowledgements

We are grateful to Jose-Ignacio Pascual, Juan José Sáenz and Carlos Bustamante for stimulating discussions. This work has been partially supported by CNR – Comitato Nazionale Informatica, National Science Foundation under Grant #DMR-9614848, and by the University of New Mexico, Albuquerque High Performance Computing Center.

Appendix A. Minimum resistance of a 1-D chain with coherent transport

Consider an STM junction consisting of $M+1$ sites embedded in the middle of a chain made of N sites, with $N-M-1$ sites forming the bath, and $N\to\infty$; the tip is the $N/2$ site, and the substrate is $N/2+M$, where M is the number of links; the sites are degenerate, and the nearest-neighbor matrix element is V, the motion being fully coherent. The dispersion relation is $E(k)=E_0+2V\cos k$, the on-site energy $E_0=0$ coincides with the Fermi level $E_{\rm F}$, and k may be treated as a continuous variable in the range $[0,\pi]$ provided that M is large. Also, the projected density of states at the tip (equal to that of the substrate) is

$$G_{\rm T}(E_{\rm F})=\frac{2}{\pi}\int_0^{\pi}{\rm d}k\sin^2(kN/2)\delta(2V\cos k)=\frac{1}{\pi V}.$$

From eqs. (2.5) and (4.13b) of Ref. [33], the minimum effective resistance is

$$R_{\rm eff}=\frac{\hbar}{2e^2}\frac{1}{G_{\rm T}(E_{\rm F})V}\int_0^{\pi}{\rm d}k\frac{\sin^2(Mk)}{\sin k}$$
$$=\frac{\hbar\pi}{2e^2}\int_0^{\pi}{\rm d}k\frac{\sin^2(Mk)}{\sin k}. \qquad \text{(A1)}$$

For $M=1$, we recover the inverse quantum of conductance $R_{\rm eff}=R_0=12.9$ kΩ. For $M=2$, $R_{\rm eff}=\frac{4}{3}R_0\approx 17.2$ kΩ. For a large M, the second integral

in Eq. (A1) can be expressed through the asymptotic formula [39] as

$$R_{\text{eff}} \approx \frac{\hbar\pi}{e^2}\frac{\ln(cM)}{2},$$

where the constant, $c \approx 7.1243$. The effective resistance of a 1-D chain of sites in resonance grows logarithmically with M, in particular R_{eff}/R_0 grows from ≈ 1.3 for $M=2$ to ≈ 4.4 for $M=1000$.

References

[1] R. Holm, J. Appl. Phys. 22 (1951) 569.
[2] J.G. Simmons, J. Appl. Phys. 34 (1963) 1793.
[3] G. Binnig, N. García, H. Rohrer, J.M. Soler, F. Flores, Phys. Rev. B 30 (1984) 4816.
[4] J.H. Coombs, M.E. Welland, J.B. Pethica, Surf. Sci. 198 (1988) L353.
[5] J.K. Gimzewski, R. Möller, Phys. Rev. B 36 (1987) 1284.
[6] N.D. Lang, Phys. Rev. B 36 (1987) 8173 this paper reports experimental data by the authors in Ref. [5].
[7] Y. Kuk, P.J. Silverman, J. Vac. Sci. Technol. A 8 (1990) 289.
[8] R. Berndt, J.K. Gimzewski, R.R. Schlittler, Ultramicroscopy 42–44 (1992) 528.
[9] N.D. Lang, Phys. Rev. B 37 (1988) 10395.
[10] R. Landauer, Phil. Mag. 21 (1970) 863.
[11] R. Landauer, IBM J. Res. Dev. 32 (1988) 306.
[12] M. Büttiker, Y. Imry, R. Landauer, S. Pinhas, Phys. Rev. B 31 (1985) 6207.
[13] G. Rubio, N. Agraït, S. Vieira, Phys. Rev. B 47 (1996) 12345.
[14] L. Olesen, E. Laegsgaard, I. Stensgaard, F. Besenbacher, J. Schiøtz, P. Stolze, K.W. Jacobsen, J.K. Nørskov, Phys. Rev. Lett. 72 (1994) 2251.
[15] L. Olesen, M. Brandbyge, M.R. Sørensen, K.W. Jacobsen, E. Laegsgaard, I. Stensgaard, F. Besenbacher, Phys. Rev. Lett. 76 (1996) 1485.
[16] M. Brandbyge, J. Schiøtz, M.R. Sørensen, P. Stolze, K.W. Jacobsen, J.K. Nørskov, L. Olesen, E. Laegsgaard, I. Stensgaard, F. Besenbacher, Phys. Rev. B 52 (1995) 8499.
[17] J.I. Pascual, J. Méndez, J. Gómez-Herrero, A.M. Baró, N. García, V.T. Binh, Phys. Rev. Lett. 71 (1993) 1852.
[18] J.I. Pascual, J. Méndez, J. Gómez-Herrero, A.M. Baró, N. García, U. Landman, W.D. Luedtke, E.N. Bogacheck, H.P. Cheng, Science 267 (1995) 1793.
[19] J.L. Costa-Krämers, Phys. Rev. B 55 (1997) R4875.
[20] E. Scheer, N. Agraït, J.C. Cuevas, A.L. Yeyati, B. Rudolph, A. Martín-Rodero, G. Rubio Bollinger, J.M. van Ruitenbeek, C. Urbina, Nature 394 (1998) 154.
[21] H. Mehrez, S. Ciraci, A. Buldum, I.P. Batra, Phys. Rev. B 55 (1997) R1981.
[22] J.I. Pascual, J.A. Torres, J.J. Sáenz, Phys. Rev. B 55 (1997) R16029.
[23] A. García-Martín, J.A. Lopez-Ciudad, A.J. Torres, J.I. Caamano, J.J. Sáenz, Ultramicroscopy 73 (1998) 199.
[24] A. Levy-Yeyati, A. Martín-Rodero, F. Flores, Phys. Rev. B 56 (1997) 10369.
[25] J. Cuevas, A. Levy-Yeyati, A. Martín-Rodero, Phys. Rev. Lett. 80 (1998) 1066.
[26] N.D. Lang, Phys. Rev. B 52 (1995) 5335.
[27] N.D. Lang, Phys. Rev. B 55 (1997) 4113.
[28] J.M. Krans, J.M. van Ruitenbeek, Surf. Sci. 383 (1997) L728.
[29] J. Ferrer, A. Martín-Rodero, F. Flores, Phys. Rev. B 38 (1988) 10113.
[30] C. Ciraci, E. Tekman, Phys. Rev. B 40 (1989) 11969.
[31] R. García-García, N. García, Surf. Sci. 251/252 (1991) 408.
[32] T.N. Todorov, A.P. Sutton, Phys. Rev. Lett. 70 (1993) 2138.
[33] V.M. Kenkre, F. Biscarini, C. Bustamante, Phys. Rev. B 51 (1995) 11074.
[34] F. Biscarini, C. Bustamante, V.M. Kenkre, Phys. Rev. B 51 (1995) 11089.
[35] R. García-García, J.J. Sáenz, Surf. Sci. 251/252 (1991) 223.
[36] A. Yazdani, D.M. Eigler, N.D. Lang, Science 272 (1996) 1921.
[37] M.L. Yu, N.D. Lang, B.W. Hussey, T.H.P. Chiang, W.A. Mackie, Phys. Rev. Lett. 77 (1996) 1636.
[38] V. Kalmeyer, R.B. Laughlin, Phys. Rev. B 35 (1987) 9805.
[39] D.H. Dunlap, personal communication.